Research Square

Preprints are preliminary reports that have not undergone peer review.
They should not be considered conclusive, used to inform clinical practice,
or referenced by the media as validated information.

Drought dynamics and hydro-climatic trends in the Rwenzori sub-region, western Uganda: A comparative multi-timescale SPEI assessment

Moses Marahi Tera

tera.marahi@stud.umu.ac.ug

Uganda Martyrs University

John Byalebeka

Uganda Martyrs University

Bernard Barasa

Kyambogo University

Research Article

Keywords: Drought dynamics, ENSO, Indian Ocean Dipole, Dipole Mode Index, SPEI, Rwenzori sub-region

Posted Date: November 20th, 2026

DOI: https://doi.org/10.21203/rs.3.rs-11468619/v1

License: This work is licensed under a Creative Commons Attribution 4.0 International License.
Read Full License

Additional Declarations: No competing interests reported.

Drought dynamics and hydro-climatic trends in the Rwenzori sub-region, western Uganda: A comparative multi-timescale SPEI assessment

Moses Marahi Tera[1*], John Byalebeka[1], Bernard Barasa[2]

[1]Faculty of Agriculture and Environment, Uganda Martyrs University, P.O. Box 5498, Kampala, Uganda.

[2]Department of Geography, Kyambogo University, P.O. Box 1, Kyambogo, Uganda.

[*]**Correspondence**: Moses Marahi Tera (tera.marahi@stud.umu.ac.ug)

Abstract

Drought remains a critical hydro-climatic hazard threatening agriculture, water resources, and rural livelihoods across sub-Saharan Africa, yet how localised, complex terrains modulate large-scale ocean-atmosphere interactions remain insufficiently understood. This study assesses multi-timescale drought variability and its teleconnection drivers in the Rwenzori sub-region by comparing two contrasting environments: Kasese (low-lying Albertine Rift Valley floor) and Fort Portal (elevated highlands). Using NASA POWER gridded data (1990–2020), we analysed the Standardised Precipitation Evapotranspiration Index at 6-month (SPEI-6) and 12-month (SPEI-12) timescales and applied Mann-Kendall, Sen's slope, Pettitt's change-point, and multiple linear regression analyses. The results reveal pronounced spatial heterogeneity. While the highlands exhibit a higher absolute frequency of drought months (65 at SPEI-6 and 68 at SPEI-12) than the rift valley floor (61 at SPEI-6 and 59 at SPEI-12), the low-lying terrain experiences substantially higher drought duration, severity, and peak intensity. Mann-Kendall analysis shows a significant long-term wetting shift for seasonal moisture (SPEI-6) at Kasese ($p < 0.05$), whereas highland trends remain non-significant. Pettitt's test identifies a non-significant hydro-climatic regime shift toward wetter conditions centred in 2011 at Kasese and 2012-2013 in Fort Portal ($p \geq 0.05$). Teleconnection modelling shows that ENSO has a modest, significant association with longer-timescale drought variability, particularly SPEI-12, whereas the Dipole Mode Index shows a stronger association at the SPEI-6 timescale. These findings reveal increasing regional moisture driven by gradual decadal variations rather than abrupt regime shifts, enhancing seasonal forecasting accuracy and refining topographically tailored climate adaptation strategies for vulnerable equatorial geographies.

Keywords Drought dynamics; ENSO; Indian Ocean Dipole; Dipole Mode Index; SPEI; Rwenzori sub-region.

1 Introduction

Drought is among the most pervasive and damaging hydro-climatic hazards worldwide, with profound consequences for agricultural production, water resources, ecosystem functioning, food security, and socio-economic development (Dai 2011; IPCC 2022; Dushimiyimana et al. 2026). It remains a major concern for the scientific community and policymakers alike (IPCC 2018; Ouhamdouch et al. 2020; Bahir et al. 2020). Unlike sudden-onset hazards such as floods, drought develops gradually through prolonged precipitation deficits combined with elevated atmospheric evaporative demand, making its onset difficult to detect and its impacts exceptionally long-lasting (Vicente-Serrano et al. 2010; Ahady et al. 2025). Under global warming, climate change is expected to alter the frequency, duration, and intensity of these events by modifying precipitation regimes and accelerating potential evapotranspiration (PET) (IPCC 2022; Bhardwaj and Mishra 2026; Disasa et al. 2026). These compounding stressors severely exacerbate the vulnerability of climate-dependent communities, particularly across sub-Saharan Africa (SSA) where smallholder farming systems maintain low institutional adaptive capacities (Mubiru et al. 2018; Dumisa et al. 2026).

Interestingly, equatorial East Africa often exhibits a unique "hydro-climatic paradox," where historical ground observations reveal distinct long-term wetting trends that diverge from the drying trajectories simulated by planetary general circulation models (Nicholson 2017; Schwarzwald and Seager 2024). This macro-regional complexity underscores the need for robust, multi-timescale observational modelling within highly sensitive topographic zones (Tilahun et al. 2026). Recent research indicates that drought frequencies and hydro-climatic dynamics across East Africa are becoming increasingly complex due to non-linear interactions between anthropogenic climate shifts and large-scale ocean-atmosphere circulation cells (Jury 2024; Taye and Dyer 2024). Recurrent macro-droughts over recent decades have triggered widespread crop failures, catastrophic livestock losses, and systemic water-supply stresses that non-parametric statistical trends can quantify (Babaousmail et al. 2024; Funk et al. 2015; Magara et al. 2025). Traditional indicators used to track seasonal predictability are proving structurally unstable due to complex thermodynamic shifts (Babaousmail et al. 2024). This instability became starkly apparent during

the 2024–2026 equatorial monitoring cycles, where catchments rapidly veered between moisture extremes, culminating in severe, localised dry spikes across northern and western zones (GEOGLAM 2026). These compound stressors demonstrate why treating drought as a simple, static precipitation deficit fails to capture the true magnitude of localised, multi-timescale water shortages (Taye and Dyer 2024). Consequently, characterising drought in this equatorial domain requires an integrated framework that models local geographic features alongside large-scale atmospheric teleconnections.

East Africa's convective dynamics are highly complex because regional rainfall varies with interactions among topography, the Inter-Tropical Convergence Zone (ITCZ), moisture fluxes from the Congo Basin, and large-scale oceanic modes (Palmer et al. 2023; Afolayan and Mekonnen 2026). The two dominant drivers of interannual climate variability in this space are the El Niño–Southern Oscillation (ENSO) and the Indian Ocean Dipole (IOD) (Saji et al. 1999; McPhaden et al. 2020). Historical data show that positive IOD and El Niño states often enhance convection over the western Indian Ocean, driving above-average rainfall, while La Niña and negative IOD phases typically induce severe seasonal droughts (Black et al. 2003; Kebacho et al. 2024). However, these teleconnections are not spatially uniform across equatorial landscapes, highlighting the need to decouple local topographic responses from broader macro-regional averages (Zheng et al. 2025). This localised atmospheric decoupling is further compounded by shifting sub-seasonal dynamics. Recent observations indicate that the onset, duration, and internal intensity of the primary rainy seasons are undergoing profound structural changes forced by modified moisture fluxes from the Congo Basin and the western Indian Ocean (Afolayan and Mekonnen 2026). These variations disrupt traditional bimodal agricultural calendars, making static, precipitation-only metrics insufficient for monitoring real-time agricultural drought stresses (Taye and Dyer 2024). Furthermore, because localised rising temperatures trigger severe compound extreme events, such as sudden transitions from flash droughts to high-magnitude flood shocks, characterising the exact multiscalar atmospheric evaporative demand within complex terrains is critical for establishing operational early-warning thresholds (Yuan et al. 2023; Babaousmail et al. 2024). Relying solely on macro-regional climate generalizations masks these critical, fine-scale variations.

The Rwenzori sub-region offers an ideal framework for exploring these dynamics because of its complex terrain and transitional position between the humid Congo rainforest air masses and the

drier East African monsoonal system. The region features sharp elevational gradients, encompassing the low-lying Albertine Rift Valley floor, the glaciated Rwenzori Mountains, and the elevated western Ugandan highlands, which generate substantial spatial variability in rainfall and temperature over short distances (Fiddes and Gruber 2014; Jury 2024). Importantly, recent trends reveal that rising temperatures can completely offset localised gains in absolute rainfall by accelerating potential evapotranspiration (PET), fundamentally altering the net climatic water balance (Palmer et al. 2023; Ojara et al. 2024). Furthermore, regional projections confirm that future increases in East African drought frequency and severity are primarily forced by heightened atmospheric evaporative demand rather than absolute precipitation deficits alone, implying that localised warming can override regional rainfall gains (Nguvava and Abiodun 2023).

In Uganda, where the socio-economic foundation relies heavily on rain-fed agriculture, these shifting weather fields present severe institutional and structural challenges (Mubiru et al. 2018). Despite recurrent droughts substantially affecting agricultural production and household welfare over the past three decades, previous hydro-climatic research in the Rwenzori region has focused almost exclusively on qualitative socio-ecological vulnerability assessments or localised flood hazards (Tibara et al. 2023). This leaves the long-term evolution, cumulative severity, and large-scale climatic drivers of regional drought fields poorly understood. While macro-regional assessments across East Africa frequently treat topographically complex landscapes as uniform climate zones, a significant knowledge gap persists regarding how sharp, localised elevational gradients decouple from planetary ocean-atmosphere drivers (Nicholson 2017; Camberlin 2018). Furthermore, existing hydro-climatic studies within the vulnerable Albertine Rift remain heavily fragmented, rarely integrating non-parametric trend detection, structural change-point verification, and multivariable teleconnection modelling within a single unified framework (Omondi and Lin 2023; Babaousmail et al. 2024). Consequently, the localised expressions of drought duration, intensity, and atmospheric water demand across the sharply contrasting microclimates of the Rwenzori sub-region remain structurally unquantified. By systematically comparing the low-lying rift valley floor of Kasese with the elevated highland baseline of Fort Portal, this study addresses these gaps through four specific objectives: (i) characterise long-term trends and magnitudes in localised precipitation, air temperature, and PET; (ii) model, quantify, and contrast multi-timescale drought characteristics using seasonal (SPEI-6) and annual (SPEI-12) drought metrics; (iii) determine whether regional moisture trends reflect gradual variations or sudden, abrupt hydro-climatic regime shifts using non-parametric change-point modelling; and (iv) isolate and decouple

the contemporaneous and lagged influences of Oceanic Niño Index (ONI) and Dipole Mode Index (DMI) on regional drought persistence. To achieve these objectives, we employ the Standardised Precipitation Evapotranspiration Index (SPEI) framework (Vicente-Serrano et al. 2010). Previous studies in Uganda and the wider East African region have substantially improved understanding of drought occurrence, temporal variability, and rainfall trends using indices such as the Standardised Precipitation Index (SPI), SPEI, and Palmer Drought Severity Index (PDSI) (Onyutha 2016; Hirpa et al. 2018; Uwimbabazi et al. 2022; Ojara et al. 2024). However, evidence specific to Kasese and Fort Portal within the Albertine Rift remains limited despite their high exposure to hydro-climatic extremes.

Consequently, this study provides three distinct scientific contributions to equatorial hydro-climatology. First, it achieves the topographic decoupling of teleconnections; unlike existing macro-regional assessments that group East Africa into uniform climate zones, this study systematically decouples how small-scale, contrasting relief structures fundamentally alter local expressions of global climate drivers like ENSO and IOD. Second, it provides water-balance framework validation by integrating non-parametric trend detection with multi-timescale SPEI modelling. This work validates the critical role of atmospheric evaporative demand (PET) over simple precipitation deficits in data-limited alpine zones, establishing a more realistic framework for drought monitoring under global warming. Finally, it delivers an empirical identification of regime shifts through a rigorous non-parametric change-point evaluation defining localised, synchronized hydro-climatic patterns in western Uganda, ultimately shifting the regional hazard profile from an assumed linear drying trend to a complex, multi-timescale progressive variation baseline. By bridging the gap between local topographic responses and macro-scale ocean-atmosphere circulation, these findings provide water resource managers, conservationists, and agricultural planners with localised, actionable insights required to design resilient, topographically tailored climate adaptation frameworks across SSA.

2 Materials and methods

2.1 Study area

The study was conducted in the Rwenzori sub-region, western Uganda, utilising long-term climate observations from two locations representing sharply contrasting hydro-climatic environments. Geographically, the Rwenzori sub-region forms a complex hydro-climatical transition zone

between the humid Congo Basin convective system and the drier equatorial East African monsoonal framework, resulting in substantial spatial variability in microclimate driven by complex topography and localised atmospheric circulation. The region has a distinct bimodal rainfall regime, with the first wet season in March–May (MAM) and the second, more pronounced wet season in September–November (SON).

Kasese lies on the low-lying floor of the Albertine Rift Valley (approximately 0°11'N, 30°06'E; grid centroid: 0.183°N, 30.100°E) at roughly 900 meters above sea level (UBOS 2017). The local terrain is characterised by steep elevational gradients extending from the semi-arid Rift Valley floor up to the snow-capped peaks of the Rwenzori Mountains, which exceed 5,000 meters above sea level. These features create a pronounced rain-shadow effect, keeping mean annual rainfall relatively low (700 to 900 mm on the valley floor) and mean annual temperatures high (22°C to 27°C) (Fiddes and Gruber 2014; Nicholson 2017). Conversely, Fort Portal in Kabarole District (approximately 0°40'N, 30°17'E; grid centroid: 0.667°N, 30.283°E) lies farther northeast in the elevated western Ugandan highlands. Because of its significantly higher elevation, Fort Portal has a cooler, wetter hydro-climatic baseline than the Rift floor, with annual rainfall often exceeding 1,500 mm. The geographic and topographically driven contrasts between these two nearby locations provide an ideal empirical framework to evaluate how local relief features modulate macro-scale atmospheric teleconnections (such as ENSO and the IOD) without regional climate noise distorting the baseline signal.

Although the Rwenzori sub-region spans diverse agro-ecological zones, we purposefully selected Kasese and Fort Portal to represent the extreme, topography-driven microclimatic contrasts within the Rwenzori catchment. By focusing on this specific sub-regional transect, the study isolates how sharp elevational gradients, from the semi-arid rift floor to the alpine highlands, modulate planetary ocean-atmosphere teleconnections without regional climate noise distorting the baseline signal. Fig. 1 illustrates the spatial configuration of the study locations and their respective topographic catchments.

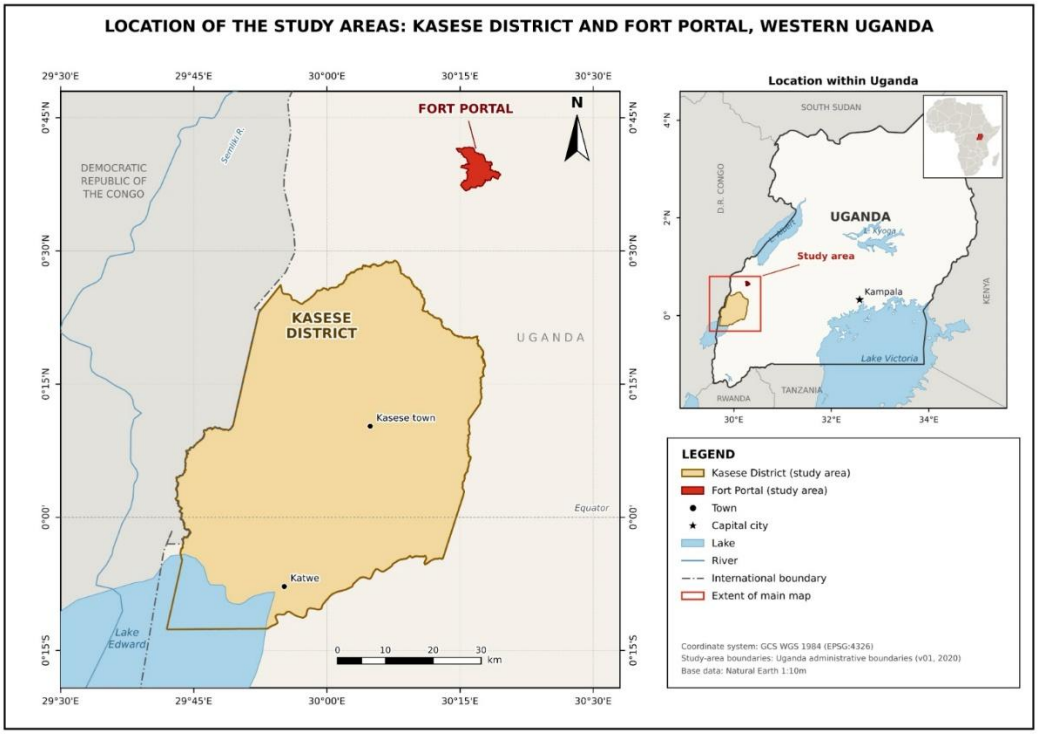


Fig. 1 Map showing the study area (Kasese and Fort Portal)

2.2 Climate data and source

The study obtained monthly precipitation and air-temperature data from January 1990 to December 2020 from the National Aeronautics and Space Administration Prediction of Worldwide Energy Resources (NASA POWER) database. The dataset comprised 31 years (372 months) of climate data for two locations in western Uganda: Kasese (0.183° N, 30.100° E) and Fort Portal (0.667° N, 30.283° E). NASA POWER is an official NASA data service that provides standardised, spatially and temporally consistent meteorological datasets derived from satellite observations and assimilation-based reanalysis products. The meteorological variables (monthly precipitation and air temperature at 2 m above the surface) used in this study originate from the Modern-Era Retrospective Analysis for Research and Applications, Version 2 (MERRA-2) produced by the NASA Global Modelling and Assimilation Office (GMAO), with a native spatial resolution of approximately 0.5° latitude × 0.625° longitude (Gelaro et al. 2017).

Before selecting the gridded database, we thoroughly investigated the physical ground-station records managed by the Uganda National Meteorological Authority (UNMA), specifically the Kasese Airfield and Fort Portal stations. However, the raw station records exhibited significant,

non-random data gaps exceeding 15% across the baseline period (particularly between 1995 and 2005), along with localised temporal inconsistencies due to historical observation interruptions. As widely documented across data-sparse equatorial domains, such extensive observation gaps severely limit the applicability of direct ground records for multi-decadal trend modelling (Mubiru et al. 2018; Hirpa et al. 2018). Because multi-timescale indices accumulate rolling atmospheric deficits over continuous mathematical steps, missing values propagate substantial errors and break the underlying parametric parameter fitting of the log-logistic probability distribution (Vicente-Serrano et al. 2010; Beguería et al. 2014). Therefore, to avoid artificial trend signals and ensure a robust, unbroken, and spatially consistent multi-decadal analysis (1990–2020), the homogenised NASA POWER reanalysis dataset was selected as the optimal macro-environmental baseline, mirroring protocols established for complex territorial downscaling (Fiddes and Gruber 2014). The selected grid centroids for Kasese (0.183° N, 30.100° E) and Fort Portal (0.667° N, 30.283° E) successfully capture the distinct sub-regional contrast between the low-lying rift valley floor and the elevated highland moisture regimes without regional climate noise distorting the baseline signals.

2.3 Methods

2.3.1 The SPEI computation

SPEI is a multiscalar drought index based on the monthly climatic water balance, calculated as the difference between precipitation (P) and potential evapotranspiration (PET). Unlike precipitation-only indices such as the Standardised Precipitation Index (SPI), SPEI explicitly incorporates atmospheric evaporative demand, providing a more physically realistic representation of drought under a warming climate (Vicente-Serrano et al. 2010; Beguería et al. 2014). This is particularly important in western Uganda, where rising temperatures may intensify drought conditions even during periods of near-normal rainfall. SPEI quantifies water deficits across multiple accumulation timescales by fitting the climatic water balance to a log-logistic probability distribution and standardizing the resulting values, thereby improving the characterisation of drought severity, duration, and intensity (Vicente-Serrano et al. 2010; Spinoni et al. 2018). SPEI remains one of the most widely applied drought indices because it incorporates both precipitation and atmospheric evaporative demand, making it particularly suitable for assessing drought under a changing climate (Nguvava and Abiodun 2023). The monthly climatic water balance (D) is expressed as:

$$D = P - PET \quad (1)$$

where D is the water surplus or deficit for the analysed month, P is the monthly precipitation accumulation and PET is the potential evapotranspiration.

We estimated monthly PET using the Thornthwaite method (Thornthwaite 1948), which is widely applied in data-limited environments because it requires minimal data (Beguería *et al*. 2014). While the Penman-Monteith formulation is widely recognized as the standard configuration for computing absolute PET, it requires comprehensive meteorological inputs (such as solar radiation, wind speed, and relative humidity) that are highly constrained or unavailable in data-sparse equatorial domains (Beguería et al. 2014). The Thornthwaite method remains highly effective for multiscalar drought monitoring in data-limited environments when the primary objective is to track relative temporal deviations in the climatic water balance rather than absolute physical energy fluxes (Vicente-Serrano et al. 2010). The accumulated different D values at different timescales (k) were fitted to a log-logistic distribution and standardised to produce SPEI values.

Thus, the computed D values are accumulated over various timescales.

$$D_n^k = \sum_{i-0}^{k-1} P_{n-1} - (PET)_{n-1} \quad (2)$$

where k is the timescale of accumulation and n is the month on which the calculation is based.

Negative SPEI values indicate drought conditions, whereas positive values represent wet conditions (McKee et al. 1993; Komuscu 1999). SPEI is computed at multiple accumulation timescales (e.g., 1, 3, 6, 9, 12, 24, and 36 months), reflecting how precipitation deficits affect different components of the hydrological cycle. The selected timescales depended on the study's objectives. In this study, 6-month (SPEI-6) and 12-month (SPEI-12) timescales were computed to analyse short- and long-term hydro-climatic drought dynamics, respectively. These timescales are well suited for assessing impacts on crop production, soil moisture, groundwater recharge, river flows, pasture availability, and lake levels which are critical for agricultural, pastoral, and fisheries systems (Vicente-Serrano et al. 2010).

2.3.2 Temporal trend analysis

We assessed temporal trends in monthly temperature, precipitation, and evapotranspiration using the MK test, a non-parametric method widely used in hydro-climatic studies because it does not assume a normal distribution of data (Mann 1945; Kendall 1975; Yue and Pilon 2004; Caloiero et

al. 2011). The MK statistic is dimensionless and does not quantify trend magnitude in the time series units; instead, it measures the correlation between a variable and time. Consequently, it indicates the direction and statistical significance of observed trends, while trend magnitude is estimated separately (Liu et al. 2021). The MK test statistic, S, is expressed as follows:

$$S = \sum_{j=1}^{n-1} \sum_{i=j+1}^{n} Sign(x_i - x_j) \quad (3)$$

where x_i and x_j are the data values at i and j, and n is the length of the dataset

$Sign\ (x_i - x_j)$ is the sign function which can be calculated as follows:

$$Sign\ (x_i - x_j) = \begin{cases} 1\ if\ (x_i - x_j) > 0 \\ 0\ if\ (x_i - x_j) = 0 \\ -1\ if\ (x_i - x_j) < 0 \end{cases} \quad (4)$$

For $n > 10$, the test statistic Z approximately follows a standard normal distribution:

$$Z = \begin{cases} \frac{S-1}{\sqrt{Var(S)}} & if\ S > 0 \\ 0 & if\ S = 0 \\ \frac{S+1}{\sqrt{Var(S)}} & if\ S < 0 \end{cases} \quad (5)$$

where $Var(S)$ denotes the variance of statistic S.

A positive Z value indicates an increasing trend, whereas a negative value indicates a decreasing trend. The null hypothesis (Ho) of no trend is accepted or rejected by comparing the computed Z statistic with the critical value from the standard normal distribution at the 5% significance level (Some'e et al., 2013). If /Z/>$Z_{(1-\alpha/2)}$, the null hypothesis of no autocorrelation and trend in the dataset is rejected, in which $Z_{(1-\alpha/2)}$ corresponds to the normal distribution, with α being the significant level. Trend magnitude was quantified using Sen's slope estimator, which computes the median of all pairwise slopes and is robust to outliers (Theil 1950; Sen 1968). Positive slope values indicate increasing wetness, whereas negative values indicate increasing dryness. We derived annual SPEI series from monthly values to reduce seasonal autocorrelation and improve the independence of observations. The magnitude of the trend can be expressed by the trend slope, β:

$$\beta = \text{Median}\left(\frac{x_i - x_j}{i - j}\right),\ \forall j < i \quad (6)$$

where x_i and x_j are data values at time t_i and t_j ($i > j$), respectively.

2.3.3 Drought identification and metrics

Table 1 shows drought events defined as SPEI ≤ −1.0, following commonly used classification thresholds (McKee *et al*. 1993). Event duration was the number of consecutive months below this threshold. We calculated severity as cumulative SPEI during the event, and intensity as severity divided by duration, representing the average drought strength per month.

Table 1 Drought classification thresholds based on SPEI indices

Index values	Classification
SPEI ≥ 2.0	Extremely wet
1.5 to 1.99	Very wet
1.0 to 1.49	Moderately wet
-0.99 to 0.99	Near normal
-1.0 to -1.49	Moderately dry
-1.5 to -1.99	Severely dry
SPEI ≤ -2.0	Extremely dry

Source: McKee et al (1993)

2.3.4 Correlation analysis

Relationships between SPEI and climatic variables were evaluated using Pearson's product-moment correlation coefficient (r). Pearson's correlation analysis was conducted to examine the strength and direction of the relationships between SPEI and the selected climatic variables; temperature, precipitation, and potential evapotranspiration (PET). Pearson correlation was selected because the variables were continuous and the objective was to quantify the strength and direction of linear associations between drought conditions and climatic drivers (Schober *et al*. 2018). The Pearson correlation coefficient (r) ranges from -1 to +1, where positive values indicate a direct relationship, negative values indicate an inverse relationship, and values closer to zero indicate weak associations (Mukaka 2012). Correlation coefficients were interpreted following Evans (1996), where r values of 0.00–0.19 indicate very weak relationships, 0.20–0.39 weak relationships, 0.40–0.59 moderate relationships, 0.60–0.79 strong relationships, and 0.80–1.00 very strong relationships.

2.3.5 Teleconnections analysis

To investigate how large-scale ocean–atmosphere variability influences drought conditions in the Rwenzori region, we incorporated ONI and DMI into the analysis. Monthly ONI data were obtained from the National Oceanic and Atmospheric Administration Climate Prediction Center (NOAA CPC 2025), where the index is defined as the three-month running mean sea surface temperature anomaly in the Niño 3.4 region (5°N–5°S, 170°–120°W). Positive ONI values indicate El Niño conditions, whereas negative values indicate La Niña conditions. Monthly DMI data were obtained from the NOAA Physical Sciences Laboratory (PSL) (NOAA PSL 2025)**.** The DMI quantifies the strength of the IOD by measuring the difference in sea surface temperature anomalies between the western equatorial Indian Ocean (50°–70°E, 10°S–10°N) and the southeastern equatorial Indian Ocean (90°–110°E, 10°S–0°). Positive DMI values represent positive IOD events associated with enhanced convection over the western Indian Ocean and increased rainfall over parts of East Africa, whereas negative values indicate the opposite phase (Saji et al., 1999).

We performed Pearson's product-moment correlation analysis to quantify contemporaneous relationships between ONI, DMI, and the SPEI-6 and SPEI-12 drought indices. Pearson's correlation coefficient measures the strength and direction of linear relationships between continuous variables (Benesty et al. 2009). Scatter plots were constructed to visualize these relationships and assess their linearity. To evaluate how drought conditions respond temporally to large-scale climate variability, we conducted cross-correlation analysis using lag periods of up to ±12 months. Cross-correlation functions quantify associations between two time series at different lags and are widely used in climatological studies to identify potential lead–lag relationships between climate drivers and hydroclimatic responses (Box et al. 2016). Positive lags indicate that variations in ONI or DMI precede changes in SPEI, whereas negative lags indicate that changes in SPEI precede variations in the climate indices. We assessed statistical significance at the 5% level ($p < 0.05$).

2.3.6 Multiple linear regression analysis

Multiple linear regression was employed to quantify the independent influence of local hydro-climatic variables and large-scale climate indices on drought variability (Montgomery et al., 2021). We developed separate regression models with SPEI-6 and SPEI-12 as dependent variables,

including monthly precipitation (PRCP), mean temperature (TMED), PET, ONI, and DMI as explanatory variables. The regression model was expressed as:

$$SPEI = \beta_0 + \beta_1 PRCP + \beta_2 TMED + \beta_3 PET + \beta_4 ONI + \beta_5 DMI + \epsilon \quad (7)$$

where β_0 is the intercept, β_1–β_5 are regression coefficients representing the effects of the explanatory variables, and ϵ is the random error term. We evaluated overall model performance using the coefficient of determination (R^2), adjusted R^2, the F-statistic, and corresponding *p*-values (Montgomery et al. 2021). Statistical significance was evaluated at the 5% level ($p < 0.05$).

2.3.7 Change-point detection

To determine whether the observed trends in drought conditions reflected gradual changes or abrupt shifts in hydro-climatic conditions, Pettitt's non-parametric change-point test was applied to the SPEI-6 and SPEI-12 time series (Pettitt 1979; Mallakpour and Villarini 2016). The test identifies a single statistically significant change point by comparing cumulative rank sums before and after each observation. The null hypothesis assumes the entire time series comes from a homogeneous distribution, whereas the alternative assumes an abrupt shift in the median at an unknown time (Pettitt 1979). We identified statistically significant change points at $p < 0.05$. To facilitate interpretation, we compared mean SPEI values before and after the detected change points to evaluate changes in drought conditions (Xie et al. 2019).

2.4 Statistical analyses

All statistical analyses were performed using R version 4.5.3. We used MK tests and Sen's slope estimators to detect monotonic trends; Pearson and cross-correlation analyses to evaluate associations among climatic variables; Pettitt's test to identify abrupt hydro-climatic regime shifts; and multiple linear regression to quantify the relative contributions of local hydro-climatic variables and large-scale climate indices to drought variability.

3 Results

3.1 Hydro-climatic characteristics and drought variability

Hydro-climatic conditions differed appreciably between the two target catchments in the Rwenzori region of western Uganda, creating a clear contrast for interpreting drought patterns. The elevated highland station of Fort Portal has a cooler, wetter climate, whereas Kasese has lower precipitation and a higher mean temperature. These differences provide an important climatic context for interpreting the spatial variability in drought characteristics identified by the SPEI. The SPEI series showed substantial interannual variability at both locations, with alternating wet and dry periods throughout the 1990–2020 study period. Both SPEI-6 and SPEI-12 identified several periods of persistent negative anomalies, indicating that drought was recurrent rather than confined to isolated years. The similarity of several major drought periods between the two stations indicates a regional component to drought variability, while differences in event duration and intensity demonstrate spatial heterogeneity in drought expression. Figs. 2 (a) and (b) show the temporal fluctuations of monthly SPEI for Kasese at the 6- and 12-month accumulation timescales, respectively, while Figs. 3 (a) and (b) present the corresponding SPEI-6 and SPEI-12 parameters for Fort Portal.

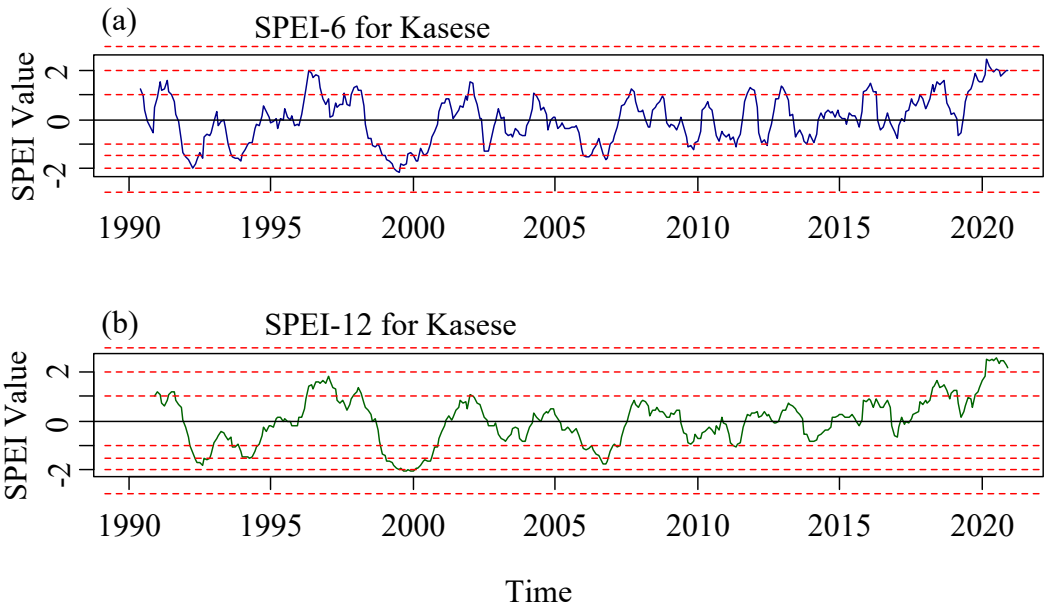


Fig. 2 Temporal fluctuations of monthly SPEI for Kasese at the (a) 6-month (SPEI-6) and (b) 12-month (SPEI-12) accumulation timescales during the historical study period (1990–2020). Dotted horizontal reference lines delineate the structural thresholds for moderate (≤ -1.0), severe (≤ -1.5), and extreme (≤ -2.0) drought conditions.

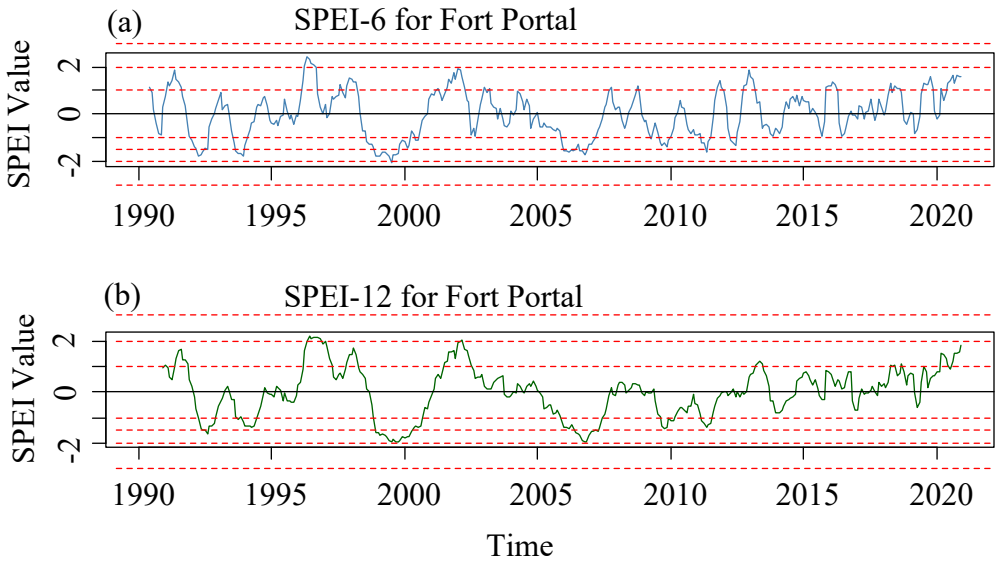


Fig. 3 Temporal fluctuations of monthly SPEI for Fort Portal at the (a) 6-month (SPEI-6) and (b) 12-month (SPEI-12) accumulation timescales during the historical study period (1990–2020). Negative vectors represent prolonged, cumulative hydrological moisture deficits, while positive columns mark baseline water surpluses.

3.2 Temporal drought characteristics

Using the standardised drought threshold of SPEI ≤ -1.0, the total number of historical drought months was found to be higher within the elevated highlands than on the rift valley floor. Fort Portal recorded 65 drought months at the short-term seasonal timescale (SPEI-6) and 68 months at the long-term hydrological timescale (SPEI-12). In comparison, the low-lying Kasese station recorded 61 and 59 drought months for the respective timescales (Table 2).

Table 2 Drought frequency, duration and severity at Kasese and Fort Portal, 1990–2020

Station	Timescale	Drought months	Drought events (≥2 months)	Longest event (months)	Minimum SPEI	Maximum cumulative severity	Dominant event
Kasese	SPEI-6	61	7	24	-2.17	37.5	1998-2000
Fort Portal	SPEI-6	65	8	20	-2.06	30.5	1998-2000
Kasese	SPEI-12	59	5	24	-2.08	41.4	1998-2000
Fort Portal	SPEI-12	68	6	22	-1.97	36.4	1998-2000

Note**:** Drought months are months with SPEI ≤ -1. Drought events are consecutive drought periods lasting ≥2 months. Cumulative severity is the sum of absolute negative SPEI values during an event.

The event analysis similarly indicated slightly more drought episodes at Fort Portal. At SPEI-6, eight multi-month drought events occurred at Fort Portal, compared with seven at Kasese (Table 2, Figs. 2a, 3a). The Fort Portal events occurred during 1992, 1993–1994, 1998–2000, 2000, 2005–2007, 2009, 2011, and 2012. Kasese recorded seven SPEI-6 events: 1991–1992, 1993–1994, 1998–2000, 2002, 2005–2006, 2006, and 2009. For SPEI-12 (Fig. 3b), six drought events were identified at Fort Portal, including prolonged episodes during 1998–2000 and 2005–2007. Kasese exhibited fewer events (Fig. 2b) but similarly identified the 1998–2000 episode as the dominant prolonged drought period. Whereas drought occurrence was somewhat more frequent at Fort Portal, drought persistence and intensity were greater at Kasese. The 1998–2000 drought is the most prominent common drought event across both locations. At SPEI-6, this event lasted approximately 24 months at Kasese (Fig. 2a) and approximately 20 months at Fort Portal (Fig. 3a). The corresponding duration–severity plots show that the event accumulated substantially greater drought severity at Kasese. The same event remains prominent at SPEI-12, lasting approximately 24 months at Kasese (Fig. 2b) and 22 months at Fort Portal (Fig. 3b). The convergence of SPEI-6 and SPEI-12 in identifying this event indicates that the 1998–2000 drought was not simply a short-lived seasonal anomaly. Rather, it represented a persistent moisture deficit operating across both intermediate and longer accumulation timescales.

At SPEI-6, Kasese reached a minimum SPEI of approximately −2.17, while Fort Portal reached approximately −2.06. For SPEI-12, the minimum values were approximately −2.08 for Kasese and −1.97 for Fort Portal. Therefore, although Fort Portal experienced slightly more drought months and events, Kasese experienced more intense minimum drought conditions and longer individual drought episodes. This shows that drought frequency alone may underestimate hazard at Kasese, because a location can have fewer drought events but still face greater risk if those events are substantially longer and more severe.

3.3 Long-term trends in hydro-climatic variables and drought indices

The MK test and Sen's slope estimates revealed contrasting long-term hydro-climatic trajectories between Kasese and Fort Portal during 1990-2020 (Table 3). The correlation results provide additional insight into the climatic controls underlying these drought-index trends.

At Kasese, precipitation exhibited a statistically significant increasing trend ($\tau = 0.347$, $Z = 2.676$, $p = 0.007$), with a Sen's slope of 12.06 mm yr^{-1}. SPEI-6 also showed a significant positive trend ($\tau = 0.301$, $Z = 2.319$, $p = 0.020$), corresponding to a Sen's slope of 0.0414 yr^{-1}, indicating a gradual shift toward wetter conditions at the six-month accumulation timescale. SPEI-12 displayed a positive but marginal trend ($\tau = 0.241$, $Z = 1.855$, $p = 0.064$), with a Sen's slope of 0.0439 yr^{-1}. In contrast, temperature ($\tau = -0.159$, $p = 0.225$), PET ($\tau = -0.154$, $p = 0.239$), ONI ($\tau = -0.083$, $p = 0.532$), and DMI ($\tau = 0.129$, $p = 0.326$) showed no statistically significant monotonic trends. Fort Portal exhibited weaker long-term changes across all variables. Precipitation showed a positive but non-significant tendency ($\tau = 0.177$, $Z = 1.356$, $p = 0.175$), with a Sen's slope of 5.88 mm yr^{-1}. SPEI-6 ($\tau = 0.159$, $p = 0.225$) and SPEI-12 ($\tau = 0.108$, $p = 0.412$) also exhibited positive but non-significant trends, with Sen's slopes of 0.0222 and 0.0182 yr^{-1}, respectively. Temperature and PET showed weak negative tendencies, but neither was statistically significant. Similarly, ONI and DMI showed no significant temporal trends. Thus, the MK analysis indicates a clearer long-term wetting tendency at Kasese, particularly for precipitation and SPEI-6, whereas the corresponding changes at Fort Portal were not statistically distinguishable from temporal variability over the study period.

Table 3 MK trend statistics, Sen's slope estimates, and Pearson correlations between local hydro-climatic variables, large-scale climate indices (ONI and DMI), and drought indices (SPEI-6 and SPEI-12) for Kasese (a) and Fort Portal (b) stations (1990 – 2020)

(a) Kasese

Variable	Tau, τ	Z	p-value	Sen's Slope	SPEI-6 (r)	SPEI-12 (r)
TEMP	-0.159	-1.213	0.2251 ns	-0.01160 °C yr^{-1}	-0.870***	-0.799***
PRCP	0.347	2.676	0.00745**	12.06 mm yr^{-1}	0.886***	0.787***
PET	-0.154	-1.178	0.2390 ns	-1.383 mm yr^{-1}	-0.874***	-0.804***
ONI	-0.083	-0.625	0.5322 ns	-0.00667 yr^{-1}	0.149 ns	0.229 ns
DMI	0.129	0.981	0.3264 ns	0.00847 yr^{-1}	0.220 ns	0.151 ns
SPEI-6	0.301	2.319	0.0204*	0.04140 yr^{-1}	--	--
SPEI-12	0.241	1.855	0.0635†	0.04387 yr^{-1}	--	--

(b) Fort Portal

Variable	Tau, τ	Z	p-value	Sen's Slope	SPEI-6 (r)	SPEI-12 (r)
TEMP	-0.0368	-0.268	0.7890 ns	-0.00188 °C yr^{-1}	-0.812***	-0.752***
PRCP	0.177	1.356	0.1751 ns	5.879 mm yr^{-1}	0.868***	0.727***
PET	-0.0391	-0.285	0.7753 ns	-0.328 mm yr^{-1}	-0.814***	-0.756***
ONI	-0.083	-0.625	0.5322 ns	-0.00667 yr^{-1}	0.237 ns	0.343†
DMI	0.129	0.981	0.3264 ns	0.00847 yr^{-1}	0.168 ns	0.033 ns
SPEI-6	0.159	1.213	0.2251 ns	0.02217 yr^{-1}	--	--
SPEI-12	0.108	0.821	0.4118 ns	0.01823 yr^{-1}	--	--

Notes: TEMP = Temperature; PRCP = Precipitation; τ = Mann–Kendall Kendall's tau; Z = standardised MK test statistic; r = Pearson correlation coefficient; PET = potential evapotranspiration; ONI = Oceanic Niño Index; DMI = Dipole Mode Index; ns = not significant ($p \geq 0.05$); † $p < 0.10$; * $p < 0.05$; ** $p < 0.01$; *** $p < 0.001$. Sen's slopes for annual variables are expressed per year. Correlations for SPEI-6 and SPEI-12 are Pearson's correlations with the respective variable. Dashes indicate that correlations of an index with itself are not applicable.

The correlation results provide additional insight into the climatic controls underlying these drought-index trends (Table 3). At Kasese, precipitation was strongly and positively correlated with SPEI-6 (r = 0.886) and SPEI-12 (r = 0.787), while PET was strongly and negatively correlated with SPEI-6 (r = −0.874) and SPEI-12 (r = −0.804). Temperature also showed strong negative correlations with SPEI-6 (r = −0.870) and SPEI-12 (r = −0.799). A comparable pattern occurred at Fort Portal, where precipitation correlated positively with SPEI-6 (r = 0.868) and SPEI-12 (r = 0.727), while PET correlated negatively with SPEI-6 (r = −0.814) and SPEI-12 (r = −0.756). Temperature showed similarly strong negative relationships with SPEI-6 (r = −0.812) and SPEI-12 (r = −0.752). These relationships show that drought variability at both locations closely tracks the balance between precipitation inputs and atmospheric evaporative demand.

3.4 Influence of ENSO and the IOD on drought variability

The relationships between the large-scale climate indices and SPEI differed by location and accumulation timescale (Table 4; Figs. 4, 5). At Kasese, ONI was positively correlated with SPEI-6 (r = 0.140, p = 0.0073, Fig. 4a) and SPEI-12 (r = 0.152, p = 0.00385, Fig. 4b). For Fort Portal, the corresponding correlations were slightly stronger, with r = 0.158 (p = 0.00233, Fig. 5a) for SPEI-6 and r = 0.229 (p < 0.001, Fig. 5b) for SPEI-12. Although statistically significant, the relatively small correlation coefficients indicate that ENSO accounted for only a modest component of the observed drought variability.

Table 4 Relationship between ENSO/IOD indices and SPEI

Relationship	Kasese		Fort Portal	
	r	p-value	r	p-value
ONI-SPEI-6	0.140	0.0073	0.158	0.00233
ONI-SPEI-12	0.152	0.00385	0.229	1.08×10^{-5}
DMI-SPEI-6	0.208	5.83×10^{-5}	0.180	0.000516
DMI-SPEI-12	0.068	0.199	0.000	0.998

The relationship with DMI depended more strongly on accumulation timescale (Table 4). At Kasese, DMI was positively correlated with SPEI-6 (r = 0.208, p < 0.001, Fig. 4c), but its association with SPEI-12 was weak and non-significant (r = 0.068, p = 0.199, Fig. 4d). Fort Portal

showed a similar pattern, with a significant positive DMI–SPEI-6 relationship ($r = 0.180$, $p = 0.000516$, Fig. 5c), but virtually no contemporaneous association between DMI and SPEI-12 ($r \approx 0$, $p = 0.998$, Fig. 5d). Thus, the contemporaneous results indicate that the ENSO signal was detectable across both accumulation timescales, with a relatively stronger association with longer-term moisture conditions at Fort Portal, whereas the DMI signal was more apparent at the six-month timescale.

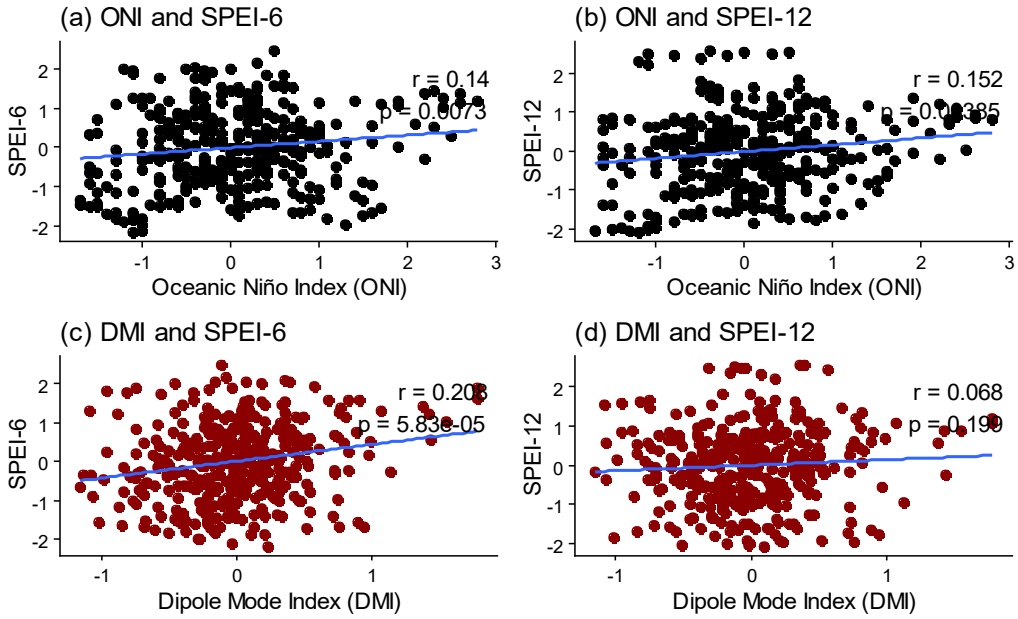


Fig. 4 Scatter plots illustrate the relationships between ONI, DMI, and drought conditions in Kasese during 1990-2020. Panels (a) and (b) show the relationships between ONI and SPEI-6 and SPEI-12, respectively, while panels (c) and (d) present the corresponding relationships for DMI. Blue lines represent fitted linear regression models, illustrating the direction of the associations between the climate indices and drought conditions.

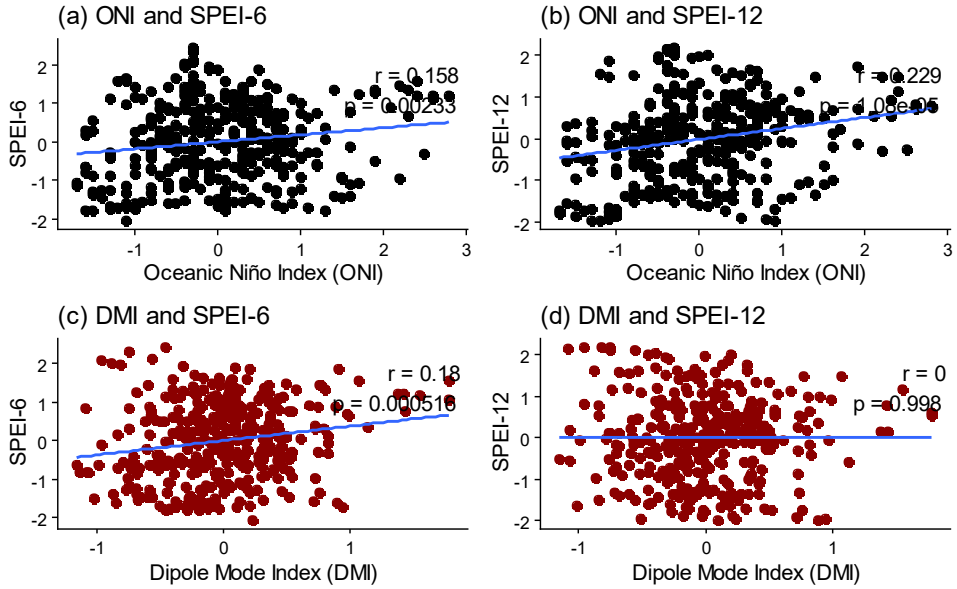


Fig. 5 Scatter plots illustrate the relationships between ONI, DMI, and drought conditions in Fort Portal during 1990-2020. Panels (a) and (b) show the relationships between ONI and SPEI-6 and SPEI-12, respectively, while panels (c) and (d) present the corresponding relationships for DMI.

3.5 Lagged relationships between climate indices and SPEI

We used cross-correlation analysis to determine whether changes in ONI and DMI preceded subsequent changes in drought conditions (Figs. 6, 7). The lagged relationships revealed additional temporal structure that was not apparent from contemporaneous correlations alone. For DMI, the relationship with SPEI-12 at Kasese increased with increasing lag and reached approximately r = 0.27 at a six-month lag (Fig. 6b), despite the weak contemporaneous association. The DMI–SPEI-6 relationship was already positive at zero lag and increased further across the examined lag periods (Fig. 6a). Fort Portal exhibited a comparable but weaker lagged response, particularly for SPEI-12 (Figs. 7a, 7b). These results indicate that the relationship between Indian Ocean variability and accumulated moisture conditions may emerge progressively rather than instantaneously.

The lagged ONI relationships similarly showed positive associations across the examined accumulation periods, although their magnitude remained relatively modest (Figs. 6c, 6d for Kasese and 7c, 7d for Fort Portal). At Fort Portal, for example, contemporaneous ONI correlations

were r = 0.158 for SPEI-6 and r = 0.229 for SPEI-12, with the latter showing a stronger relationship between the ENSO index and the longer-timescale drought indicator (Figs. 7c, 7d). At Kasese, the corresponding relationships were weaker but remained statistically significant (Figs. 6c, 6d). Overall, the lagged analysis suggests that drought responses to large-scale climate variability depend not only on the magnitude of the climate anomaly but also on the time scale over which moisture deficits accumulate.

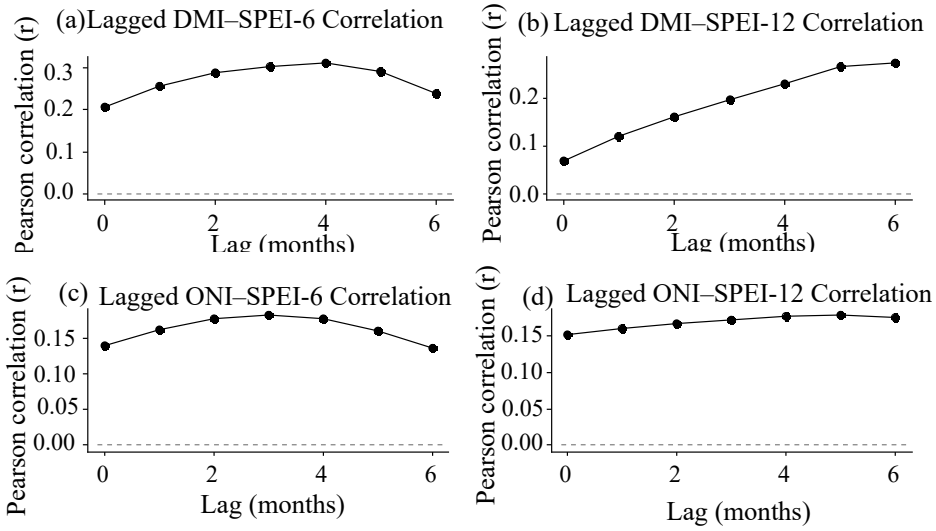


Fig. 6 Line charts illustrate contemporaneous cross-correlation functions (CCF) and lagged lead-lag coefficients (up to ± 12 months) between oceanic teleconnection indices and multi-timescale drought anomalies for Kasese.

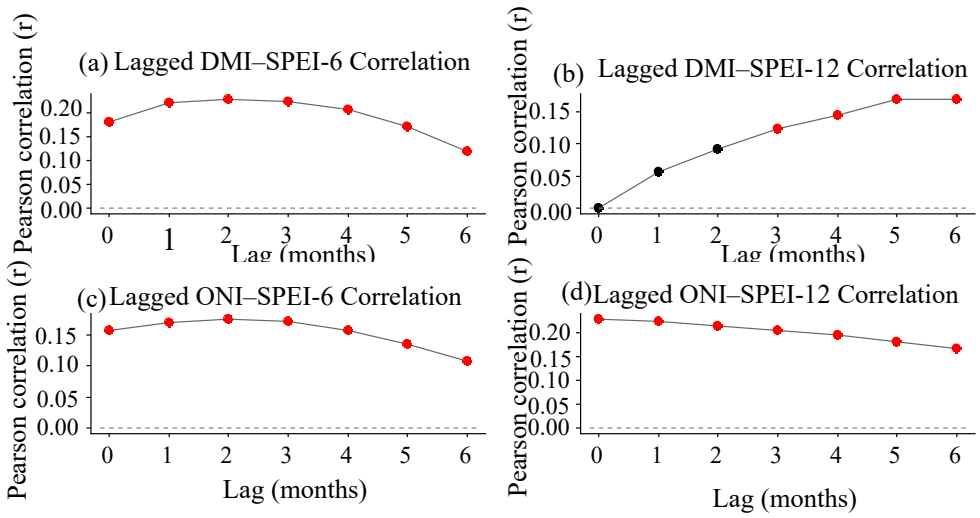


Fig. 7 Line charts illustrate contemporaneous cross-correlation functions (CCF) and lagged lead-lag coefficients (up to ±12 months) between oceanic teleconnection indices and multi-timescale drought anomalies for Fort Portal.

3.6 Multiple regression analysis of climatic controls on drought variability

We then used multiple linear regression to evaluate the independent contributions of precipitation, mean temperature, PET, ONI, and DMI to SPEI variability after accounting for the other predictors (Table 5).

Multiple linear regression showed that combined hydro-climatic and large-scale climate predictors significantly explained variability in SPEI-6 and SPEI-12 at Kasese and Fort Portal (Table 5, $p < 0.001$). The models explained 29.0% and 21.4% of SPEI-6 and SPEI-12 variability at Kasese, respectively, compared with 24.9% and 21.0% at Fort Portal. Precipitation was consistently and positively associated with SPEI across both locations and timescales, while PET exhibited a significant negative association in all models. In contrast, mean temperature was not independently significant in any model, despite its strong bivariate correlations with SPEI (Table 3). This suggests that atmospheric evaporative demand largely captured its contribution to drought variability.

Table 5 Multiple linear regression models explaining drought variability (SPEI-6 and SPEI-12) in Kasese (a) and Fort Portal (b)

(a) Kasese

Predictor	SPEI-6 β	t	p-value	SPEI-12 β	t	p-value
Intercept	3.1457	1.249	0.2126 ns	3.0653	1.148	0.2518 ns
PRCP	0.00378	3.645	<0.001***	0.00291	2.610	0.009***
TMED	0.01548	0.087	0.9307 ns	0.01043	0.055	0.956 ns
PET	−0.04399	−2.433	0.0155*	−0.04095	−2.138	0.033*
ONI	0.10023	1.874	0.0617†	0.17236	3.039	0.0025**
DMI	0.20908	2.144	0.0327*	−0.11763	−1.119	0.264 ns
R^2	0.2899			0.2138		
Adjusted R^2	0.2800			0.2028		
F-statistic	29.47			19.31		
Model p-value	$<2.2x10^{-16*}$			$<2.2x10^{-16*}$		

(b) Fort Portal

Predictor	SPEI-6 β	t	p-value	SPEI-12 β	t	p-value
Intercept	2.6309	1.280	0.2012 ns	3.3821	1.590	0.1127 ns
PRCP	0.00394	4.540	<0.001***	0.00219	2.407	0.0166*
TMED	0.06471	0.377	0.7063 ns	0.02463	0.139	0.8894 ns
PET	−0.05803	−2.690	0.0075*	−0.05471	−2.461	0.0143*
ONI	0.12039	2.189	0.0292*	0.28607	5.040	<0.001***
DMI	0.20860	2.098	0.0366*	−0.25116	−2.411	0.0164*
R^2	0.2486			0.2104		
Adjusted R^2	0.2382			0.1992		
F-statistic	23.89			18.92		
Model p-value	$<2.2x10^{-16*}$			$<2.2x10^{-16*}$		

Notes: β = unstandardised regression coefficient; *t* = Student's *t*-statistic; PRCP = precipitation; TMED = mean temperature; PET = potential evapotranspiration; ONI = Oceanic Niño Index; DMI = Dipole Mode Index; ns = not significant ($p \geq 0.05$); † $p < 0.10$; * $p < 0.05$; ** $p < 0.01$; *** $p < 0.001$.

The influence of the large-scale climate indices varied with accumulation timescale and location. At Kasese, ONI was marginally associated with SPEI-6 (β = 0.100, p = 0.062) but became significant for SPEI-12 (β = 0.172, p = 0.003). At Fort Portal, ONI was significant for both SPEI-6 (β = 0.120, p = 0.029) and SPEI-12, with a substantially stronger association at the annual

timescale ($\beta = 0.286$, $p < 0.001$). DMI was positively associated with SPEI-6 at both Kasese ($\beta = 0.209$, $p = 0.033$) and Fort Portal ($\beta = 0.209$, $p = 0.037$), whereas its SPEI-12 relationship was non-significant at Kasese but negative and significant at Fort Portal ($\beta = -0.251$, $p = 0.016$). Overall, the association of ENSO with drought variability was generally stronger at the longer SPEI-12 accumulation timescale, whereas DMI showed a more pronounced relationship with SPEI-6 and considerable spatial and timescale dependence.

3.7 Change-point analysis of drought indices

To test whether temporal variability in drought conditions was associated with abrupt shifts in hydro-climatic regimes, we applied Pettitt's non-parametric change-point test to the SPEI-6 and SPEI-12 time series for both locations (Table 6). The analysis showed that neither environment experienced a statistically significant, abrupt structural regime shift over the 1990-2020 study period, indicating that observed changes reflect gradual hydro-climatic variation rather than sharp baseline breaks ($p \geq 0.05$).

Table 6 Pettitt change-point analysis for drought indices in Kasese and Fort Portal (1990–2020)

Timescale	Location	Change-year	Pettitt U*	p-value	Pre- mean	Post-mean	Mean change
SPEI-6	Kasese	2011	104	0.2424	−0.194	0.504	0.698
SPEI-12	Kasese	2011	98	0.3071	−0.199	0.588	0.787
SPEI-6	Fort Portal	2013	86	0.4724	−0.115	0.405	0.520
SPEI-12	Fort Portal	2012	70	0.7688	−0.114	0.416	0.530

At Kasese, the Pettitt test identified candidate change points in July 2011 for SPEI-6 and September 2011 for SPEI-12, though neither was statistically significant (Table 6; Fig. 8a, 8b). Although there was no abrupt statistical break, these markers indicate a visible transition phase: for Kasese SPEI-6, mean index values rose from −0.194 in the pre-change period to 0.504 post-change, representing a substantial increase in moisture balance of 0.698. Similarly, the Kasese SPEI-12 mean values shifted from −0.199 to 0.588 following the September 2011 breakpoint, yielding a net positive balance shift of 0.787.

A comparable non-significant pattern was observed at Fort Portal, although the estimated change points occurred slightly later (Table 6; Figs. 9a, 9b). The SPEI-6 series indicated a change point in 2013, with the mean index values increasing from −0.115 before the change point to 0.405 afterwards, a difference of 0.520. For SPEI-12, the estimated change point occurred in 2012, with the mean index values rising from −0.114 to 0.416, representing a difference of 0.530. Because all calculated Pettitt test statistics yielded p-values well above the standard 5% significance level ($p = 0.242$ to 0.769), we cannot reject the null hypothesis of a homogeneous distribution. Consequently, the observed regional trends toward a more positive moisture balance should be interpreted strictly as evidence of gradual hydro-climatic variations rather than definitive, sudden regime transitions.

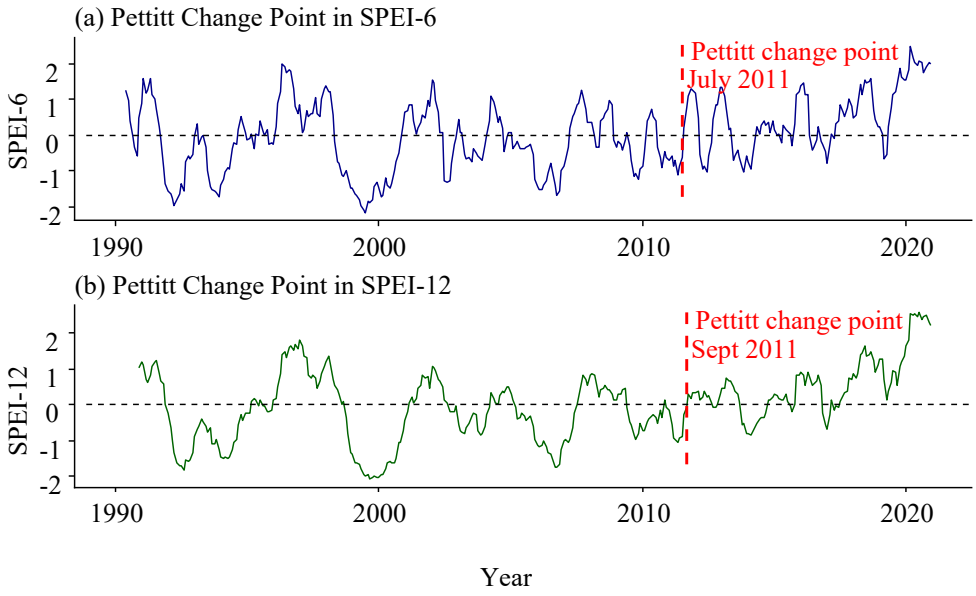


Fig. 8 Pettitt change-point analysis of (a) SPEI-6 and (b) SPEI-12 for Kasese (1990–2020). Red dashed vertical lines indicate the change points detected in July 2011 (SPEI-6) and September 2011 (SPEI-12), marking the transition from predominantly drier to wetter hydroclimatic conditions.

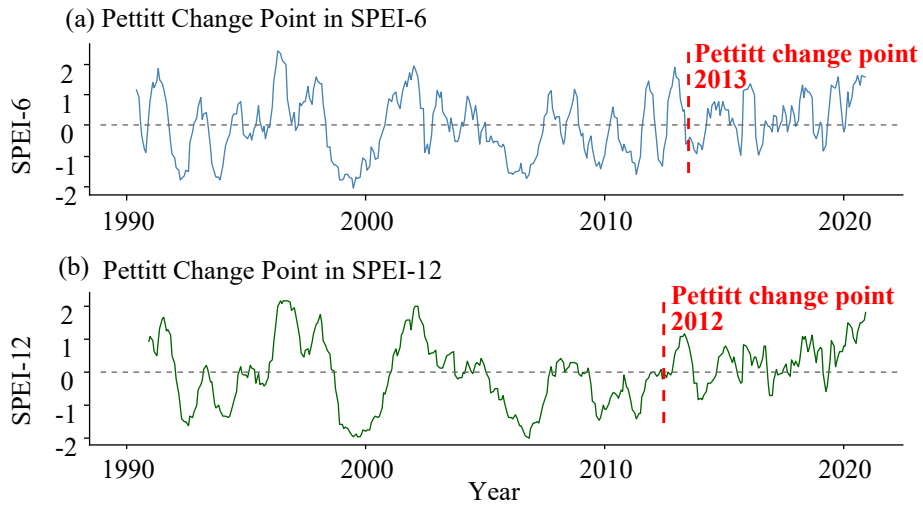


Fig. 9 Pettitt change-point analysis of (a) SPEI-6 and (b) SPEI-12 for Fort Portal (1990–2020). Blue dashed vertical lines indicate the mathematically calculated change points in 2013 (SPEI-6) and 2012 (SPEI-12), which remain statistically non-significant ($p \geq 0.05$), representing a gradual hydro-climatic variation rather than an abrupt regime shift.

4 Discussion

The multi-timescale analysis of drought dynamics in the Rwenzori sub-region during 1990–2020 reveals a substantial temporal and spatial variability in moisture conditions between the Albertine Rift Valley floor (Kasese) and the elevated western highlands (Fort Portal). The positive SPEI trend, particularly at Kasese, indicates a shift toward increasingly positive moisture-balance conditions in the latter part of the study period. This observed wetting tendency contrasts with the expectation of generalised drying in some tropical and subtropical regions under climate change and reinforces the importance of regional hydro-climatic heterogeneity in equatorial Africa (Dai 2013; Spinoni et al. 2018). The results align with the broader recognition that climate change does not produce spatially uniform drought responses, as precipitation variability, atmospheric evaporative demand, topography, and large-scale circulation interact to produce contrasting local outcomes (Vicente-Serrano et al. 2010; Nicholson 2017). Furthermore, the positive SPEI trajectory in Kasese is consistent with the heterogeneous hydro-climatic behaviour documented across equatorial East Africa, where observed precipitation and moisture balance trends may diverge from broader expectations of drying (Nicholson 2017; Schwarzwald and Seager 2024). The comparison between Kasese and Fort Portal further demonstrates that locations within relatively short geographical distances can exhibit different drought characteristics, highlighting the importance

of local physiography when interpreting regional drought signals (Tilahun et al. 2026; Wibawanty et al. 2026).

The drought-event analysis provides particularly important evidence of this spatial differentiation. Although the cooler, higher terrain of Fort Portal experienced more drought months at the SPEI-12 timescale (68 months) than Kasese (59 months), the low-lying Rift Valley floor of Kasese was prone to significantly more severe, intense, and prolonged individual macro-drought events. The most notable example was the 1998–2000 episode, which persisted for approximately 24 months at Kasese and produced a substantial cumulative moisture deficit. This distinction shows that drought frequency alone does not capture drought risk. Locations with relatively frequent but shorter moisture deficits may face different ecological and agricultural consequences than areas with fewer but substantially longer, more severe drought episodes (Chiang et al. 2021). These differences align with previous studies showing that drought characteristics vary considerably across heterogeneous African landscapes because of differences in elevation, rainfall regimes, land-surface conditions, and moisture persistence (Masih et al. 2014; Van Loon 2015; Ojara et al. 2024). For agricultural systems, prolonged drought persistence may be particularly consequential because it can progressively deplete soil moisture, water resources and household coping capacity even when the total number of drought events is relatively low (Chiang et al. 2021; Bhardwaj and Mishra 2026).

Multivariable linear regression models further indicate that drought variability was associated with both local hydro-climatic conditions and large-scale climate variability. PET emerged as an important negative predictor of SPEI across the fitted models. This result is physically consistent with the SPEI formulation, which incorporates atmospheric evaporative demand into the climatic water balance. PET therefore provides information about atmospheric water demand that precipitation alone cannot capture. This finding supports broader evidence that increasing evaporative demand can intensify moisture stress even when precipitation does not decline substantially (Vicente-Serrano et al. 2010; Beguería et al. 2014). The loss of mean temperature's independent significance when PET was included should not be interpreted as evidence that temperature is unimportant; rather, it suggests that much of temperature's influence on SPEI may be expressed through its contribution to atmospheric evaporative demand. This further justifies using SPEI as a water-balance-based drought indicator in environments where temperature and moisture demand change simultaneously (Beguería et al. 2014). This localised statistical behaviour

718 strongly aligns with the wider regional modelling of Nguvava and Abiodun (2023), who
719 demonstrated that future East African drought modes are overwhelmingly dominated by enhanced
720 surface evaporative losses rather than changing rain baselines.

721 Furthermore, the teleconnection demonstrates that large-scale climate drivers operate differently
722 across accumulation timescales and locations. ONI exhibited stronger relationships with the
723 longer-term SPEI-12 series, with positive coefficients in both Kasese and Fort Portal. This is
724 consistent with evidence that ENSO-related circulation anomalies influence rainfall variability
725 across East Africa and can contribute to wetter conditions during El Niño events and drier
726 conditions during some La Niña episodes (Vicente-Serrano et al. 2011a; McPhaden et al. 2020;
727 Magara et al. 2025). The stronger association at the annual accumulation timescale suggests that
728 Pacific Ocean variability may be particularly relevant when assessing cumulative moisture
729 conditions rather than individual seasonal anomalies. Nevertheless, interpret the relationship as a
730 statistical association rather than direct causation, because ENSO impacts are mediated through
731 regional atmospheric circulation and may vary by season and location. In contrast, DMI showed a
732 stronger association with shorter-term SPEI variability, suggesting that Indian Ocean conditions
733 may contribute more directly to seasonal moisture fluctuations. The divergent DMI response at the
734 SPEI-12 timescale is particularly notable: its relationship was not statistically significant at Kasese
735 but was negative and significant at Fort Portal ($\beta = -0.251$, $p = 0.0164$). This difference shows
736 that Indian Ocean variability does not affect rainfall uniformly, even within the Rwenzori sub-
737 region western Uganda. The contrasting responses may reflect differences in elevation, local
738 rainfall regimes and land–atmosphere interactions between the Albertine Rift environment and the
739 higher-elevation Fort Portal setting. Similar spatial and temporal heterogeneity in the influence of
740 Indian Ocean variability has been documented across East Africa (Black et al. 2003; Nsubuga et
741 al. 2014; Kebacho et al. 2024; Zheng et al. 2025). These results emphasise the value of considering
742 both ENSO and IOD information when developing locally relevant seasonal and interannual
743 drought-monitoring systems (Tan et al. 2026).

744 The Pettitt change-point test demonstrates that this regional wetting shift was not a gradual, linear
745 drift or an abrupt climate shock, but rather a gradual, statistically non-significant regime shift
746 across both terrains ($p \geq 0.05$). Both Kasese (centered in 2011) and Fort Portal (centered around
747 2012–2013) demonstrated descriptive shifts toward positive mean SPEI scores, but neither
748 baseline transition crossed the threshold of true statistical structural breakpoints. This indicates a

highly synchronised but progressive regional adjustment to changing climate inputs rather than localised atmospheric decoupling. While this gradual wetting shift has altered the immediate hazard profile toward excess moisture, long-term multi-ensemble projections at specific 1.5 °C and 2 °C global warming tiers caution that intense, multi-timescale drought modes will still pose severe structural threats across broader East African catchments (Nguvava and Abiodun 2023; Taye and Dyer 2024). Post-break years show a shift to positive mean SPEI scores, consistent with the expanding historical record of flash floods, landslides, and river overflows along the slopes of the Rwenzori Mountains (Tibara et al. 2023; Jury 2024). Furthermore, the apparent transition towards wetter drought-index conditions should not necessarily be interpreted as a reduction in overall hydro-climatic risk (Roy and Troccoli 2024). A wetter mean moisture balance can coexist with increased variability and more frequent high-intensity rainfall events. Western Uganda, particularly the Rwenzori sub-region, has steep terrain and strong topographic gradients that can amplify the consequences of intense rainfall through rapid runoff, flooding, erosion, and landslides (Tibara et al. 2023; Yuan et al. 2023; Jury 2024). Consequently, reduced drought duration does not automatically translate into reduced agricultural or livelihood vulnerability. Instead, the hazard profile may become increasingly characterised by alternating periods of moisture surplus and deficit. This finding has important implications for climate-risk management because drought monitoring should be integrated with flood and extreme-rainfall early-warning systems rather than treated as a stand-alone intervention (Wainwright et al. 2024; WMO 2025).

Taken together, the findings demonstrate that drought dynamics in the Rwenzori sub-region, are governed by interactions among local atmospheric water demand, precipitation variability, large-scale oceanic forcing and heterogeneous terrain. The contrast between Kasese and Fort Portal shows that regional-scale climate signals can manifest differently at individual locations. The results therefore support a multi-timescale, context-specific approach to drought monitoring, in which SPEI is complemented by information on PET, ENSO, and IOD conditions. For agricultural planning, the findings also suggest that early-warning systems should distinguish between short-term seasonal moisture anomalies and longer-term accumulated water-balance conditions. Such an approach would provide a stronger basis for anticipatory agricultural planning, water-resource management and climate-resilience interventions in western Uganda.

While this study provides important, localised insights into equatorial drought dynamics, certain limitations must be acknowledged. First, reliance on homogenised satellite-derived reanalysis data

from the NASA POWER database, driven by extensive gaps in regional ground-station records, may smooth out extreme microclimatic gradients across the Albertine Rift's complex topography. As highlighted by Fiddes and Gruber (2014), grid-box averages cannot fully capture the discrete micro-climatic point variations typical of steep alpine terrain. Future studies should prioritise high-resolution dynamically downscaled climate products or localised gauge-blended datasets to better capture fine-scale boundary layer variations. Second, computing PET via the temperature-dependent Thornthwaite formulation, though highly reliable for tracking relative deviations in data-sparse domains, omits wind speed, relative humidity, and solar radiation inputs. Integrating the standard Penman-Monteith configuration will refine absolute physical energy fluxes as comprehensive meteorological inputs become available (Beguería et al. 2014). Finally, while this work successfully decouples linear ocean-atmosphere teleconnections using ONI and DMI at specific lag phases, exploring non-linear predictive frameworks and multi-ensemble regional climate model projections at specific global warming tiers remains a vital frontier for sharpening seasonal early-warning systems in highly vulnerable equatorial landscapes.

5 Conclusion

This study provides a multi-timescale characterisation of drought dynamics and hydro-climatic trends in the Rwenzori sub-region, western Uganda, during 1990-2020, comparing the contrasting environments of Kasese and Fort Portal. The findings demonstrate substantial spatial and temporal heterogeneity in drought characteristics. Although Fort Portal recorded more drought months at the SPEI-12 timescale, Kasese experienced more persistent and severe drought conditions, including the prolonged 1998–2000 episode. This demonstrates that drought frequency alone is insufficient for assessing drought risk and should be considered alongside duration, persistence and severity. The trend analysis indicates an overall tendency towards more positive SPEI conditions, particularly at Kasese. PET emerged as an important negative predictor of SPEI in multivariable models. This highlights the importance of atmospheric evaporative demand in drought development and supports using water-balance-based indicators such as SPEI rather than precipitation-only indices for drought monitoring.

Pettitt change-point analysis confirmed that neither location experienced a statistically significant, abrupt hydro-climatic regime shift over the study period ($p \geq 0.05$). Candidate change points detected in Kasese around mid-2011 and in Fort Portal around 2012–2013 remained well above

the standard 5% significance level, demonstrating that the regional shift toward a more positive moisture balance represents a gradual, multi-timescale hydro-climatic transition rather than sudden baseline breaks. Incorporating ENSO and IOD information into drought-monitoring systems could therefore improve seasonal and interannual climate-risk assessment, as ONI exhibited stronger associations with longer-term SPEI-12 variability, whereas DMI was more relevant to shorter-term SPEI-6 conditions.

Overall, the findings emphasise that increasingly positive moisture conditions do not necessarily imply reduced climate risk. Drought conditions may coexist with intense rainfall, flooding, erosion and landslide hazards in the topographically complex landscapes of the Rwenzori sub-region in western Uganda. Climate-resilience planning should therefore integrate drought and excess-moisture hazards through multi-timescale SPEI monitoring, PET assessment, ENSO and IOD information, and localised early-warning systems. Such integrated approaches can strengthen agricultural planning, water-resource management and disaster-risk reduction under increasing hydro-climatic variability.

Author contributions Tera Marahi Moses: Conceptualisation, Methodology, Data curation, Formal analysis, Software, Investigation, Visualization, Writing – original draft, Writing – review & editing. John Byalebeka: Conceptualisation, Methodology, Supervision, Validation, Writing – review & editing. Barasa Bernard: Conceptualisation, Methodology, Supervision, Validation, Writing – review & editing.

Acknowledgements The authors gratefully acknowledge the INTERVENE Scholarship Program of the International Institute for Applied Systems Analysis (IIASA) and the Lake Victoria Basin Commission (LVBC) for the financial and scientific support provided during this research. Appreciation is also extended to the INTERVENE research team and Community of Practice for the training opportunities, webinars, and scientific discussions that strengthened the quality of this study.

Funding The INTERVENE Scholarship Program, implemented by the International Institute for Applied Systems Analysis (IIASA) in partnership with the Lake Victoria Basin Commission (LVBC) and funded by the Austrian Development Cooperation (ADC) under Fee Contract No. FC 250053. The scholarship supported the study's data analysis and scientific advancement. The

funders had no role in the study design, data collection, interpretation of the results, manuscript preparation, or the decision to publish.

Conflicts of interest The authors declare no conflicts of interest.

Data availability statement The climate data used in this study are publicly available through the NASA POWER database (https://power.larc.nasa.gov/data-access-viewer/). Derived datasets and analytical scripts used are available from the corresponding author upon reasonable request.

References

Afolayan S, Mekonnen A (2026) Sub-Seasonal Rainfall Variability and Atmospheric Dynamics During East African Long-Rain. Atmosphere 17(1):85. https://doi.org/10.3390/atmos17010085

Ahady AB, Klopries EM, Schüttrumpf H, Wolf S (2025) Drought analysis methods: a multidisciplinary review with insights on key decision-making factors in method selection. Water 17(15):2248. https://doi.org/10.3390/w17152248

Babaousmail H, Benabdelouahab T, El Morhit M, El Garouani A (2024) Quantifying drought impacts based on the reliability–resiliency–vulnerability framework over East Africa. Climate, 12(7):92. https://doi.org/10.3390/cli12070092

Bahir M, Ouhamdouch S, Ouazar D, El Mocayd N (2020) Climate Change Effect on Groundwater Characteristics within Semi-Arid Zones from Western Morocco. Groundwater for Sustainable Development, 11:100380. https://doi.org/10.1016/j.gsd.2020.100380

Beguería S, Vicente-Serrano SM, Reig F, Latorre B (2014) Standardized precipitation evapotranspiration index (SPEI) revisited: Parameter fitting, evapotranspiration models, tools, datasets and drought monitoring. International Journal of Climatology 34:3001–3023. https://doi.org/10.1002/joc.3887

Benesty J, Chen J, Huang Y, Cohen I (2009) Pearson correlation coefficient. In Noise Reduction in Speech Processing. Springer, Berlin/Heidelberg, pp 1-4. https://doi.org/10.1007/978-3-642-00296-0_5 .

Bhardwaj K, Mishra A (2026) Droughts in a warming climate: projected changes, sectoral impacts, and adaptation challenges. Stoch Environ Res Risk Assess 40:160. https://doi.org/10.1007/s00477-026-03296-x

Black E, Slingo JM, Sperber KR (2003) An observational study of the relationship between excessively strong short rains in coastal East Africa and Indian Ocean sea surface temperatures. Monthly Weather Review, 131(1):74–94. https://doi.org/10.1175/1520-0493(2003)131<0074:AOSOTR>2.0.CO;2 .

Box GEP, Jenkins GC, Reinsel GC, Ljung GM (2016) Time Series Analysis: Forecasting and Control, 5th edn. John Wiley & Sons, New York.

Caloiero T, Coscarelli R, Ferrari E, Mancini M (2011) Trend detection of annual and seasonal rainfall in Calabria (Southern Italy). Int J of Climatol 31: 44-56. https://doi.org/10.1002/joc.2055

Camberlin P (2018) Climate of Eastern Africa. In: Oxford Research Encyclopedia of Climate Science. Oxford University Press, Oxford. https://doi.org/10.1093/acrefore/9780190228620.013.512

Chiang F, Mazdiyasni O, AghaKouchak A (2021) Evidence of anthropogenic impacts on global drought frequency, duration, and intensity. *Nat Commun* 12:2754. https://doi.org/10.1038/s41467-021-22314-w.

Dai A (2011) Drought under global warming: A review. WIREs Clim Change 2:45–65. https://doi.org/10.1002/wcc.81

Dai A (2013) Increasing drought under global warming in observations and models. Nat Clim Change 3:52–58. https://doi.org/10.1038/nclimate1633

Disasa KN, Yan H, Zhang J, Wang G, Zhang C, Zhang D, Wang B, Hao B (2026) Comprehensive review of drought characteristics and intensification under climate change: implications for agriculture and water resources. J Hydrol 664(Part C):134571. https://doi.org/10.1016/j.jhydrol.2025.134571

Dumisa BM, Ndwandwe N, Khumalo NZ, Sibanda M (2026) Climate adaptation for small-scale farmers in Sub-Saharan Africa: a systematic review of challenges, practices, and policy gaps. Sustainability 18(16):8216. https://doi.org/10.3390/su18168216

Dushimiyimana C, Ngango J, Maniriho A (2026) Climate change impacts on agricultural productivity and resilience in Sub-Saharan Africa. Discov Sustain 7:1640. https://doi.org/10.1007/s43621-026-03984-2.

Evans JD (1996) Straightforward statistics for the behavioral sciences. Brooks/Cole Publishing.

Fiddes J, Gruber S (2014) TopoSCALE v1.0: Downscaling gridded climate data in complex terrain. Geosci Model Dev 7(2):387–405. https://doi.org/10.5194/gmd-7-387-2014

Funk C, Peterson P, Landsfeld M, Pedreros D, Verdin J, Shukla S, Husak G, Rowland J, Harrison L, Hoell A, Michaelsen J (2015) The climate hazards infrared precipitation with stations-A new environmental record for monitoring extremes. Sci Data 2:150066. https://doi.org/10.1038/sdata.2015.66

Gelaro R, McCarty W, Sua'rez MJ, Todling R, Da Silva A, Sentellas PC, Zhao B (2017) The Modern-era retrospective analysis for research and applications, version 2 (MERRA-2). J Clim 30(14):5419-5454. https://doi.org/10.1175/JCLI-D-16-0758.1

GEOGLAM (2026) GEOGLAM Global Crop Monitor. No. 48, October 2026. cropmonitor.org. Accessed 19 Oct 2026

Hirpa FA, Dyer E, Hope R, Olago DO, Dadson SJ (2018) Finding sustainable water futures in data-sparse regions under climate change: Insights from the Turkwel River basin, Kenya. J Hydrol Reg Stud 19:124-135. https://doi.org/10.1016/j.ejrh.2018.08.005

IPCC (2018) Summary for Policymakers, Global Warming 1.5 ˚C, IPCC Special Report on the Consequences of Global Warming 1.5 ˚C Relative to Pre-Industrial Levels and Associated Pathways of Global Gas Emissions Greenhouse Effect. World Meteorological Organization, Geneva, p 32

IPCC (2022) Climate Change 2022: Impacts, Adaptation and Vulnerability. Contribution of Working Group II to the Sixth Assessment Report of the Intergovernmental Panel on Climate Change. Cambridge University Press, Cambridge/New York. https://doi.org/10.1017/9781009325844

Jury MR (2024) Climate variability and hydrology impacts in East Africa's Rwenzori Mountains. J Hydrol Reg Stud 55:101922. https://doi.org/10.1016/j.ejrh.2024.101922

Kebacho LL, Ongoma V, Chen H (2024) Influence of ENSO, Southern Annular Mode, and Indian Ocean Dipole on the interdecadal change of East African short rains. Clim Dyn 62:4315–4329. https://doi.org/10.1007/s00382-024-07136-y

Kendall MG (1975) Rank correlation methods, 4th edn. Griffin, London.

Komuscu AU (1999) Using the SPI to Analyse Spatial and Temporal Patterns of Drought in Turkey. Drought Netw News 11:7-13

Liu C, Yang C, Yang Q, Wang J (2021) Spatiotemporal drought analysis by the standardized precipitation index (SPI) and standardized precipitation evapotranspiration index (SPEI) in Sichuan Province, China. Sci Rep 11:5643. https://doi.org/10.1038/s41598-020-80527-3

Magara G, Okrah A, Yao YIS, Yeboah E, Darko G, Akimana D, Sarfo I (2025) A Quantitative Assessment of Drought Trends in Uganda Using Statistical Models for Hydrological Indicators. Int J Environ Clim Change 15(2):517–537. https://doi.org/10.9734/ijecc/2025/v15i24744

Mallakpour I, Villarini G (2016) A simulation study to examine the sensitivity of the Pettitt test to detect abrupt changes in mean. Hydrol Sci J 61(2):245–254. https://doi.org/10.1080/02626667.2014.981502

Mann HB (1945) Nonparametric tests against trend. Econometrica, 13:245–259.

Masih I, Maskey S, Mussá F, Trambauer P (2014) A review of droughts on the African continent: A geospatial perspective. Hydrol Earth Syst Sci 18:3635–3649. https://doi.org/10.5194/hess-18-3635-2014.

McKee TB, Doesken NJ, Kleist J (1993) The relationship of drought frequency and duration to time scales. In: Proceedings of the 8th Conference on Applied Climatology, Anaheim, pp 179–184

McPhaden MJ, Santoso A, Cai W (Eds.) (2020) El Niño–Southern Oscillation in a changing climate. Wiley, Hoboken. https://doi.org/10.1002/9781119548164

Montgomery DC, Peck EA, Vining GG (2021) Introduction to Linear Regression Analysis, 6th edn. John Wiley & Sons, Hoboken

Mubiru DN, Radeny M, Kyazze FB, Zziwa A, Lwasa J, Kinyangi J, Mungai C (2018) Climate trends, risks and coping strategies in smallholder farming systems in Uganda. Clim Risk Manage 22:4–21. https://doi.org/10.1016/j.crm.2018.08.004

Mukaka MM (2012) Statistics corner: A guide to appropriate use of correlation coefficient in medical research. Malawi Med J 24(3):69–71. https://www.ncbi.nlm.nih.gov/pmc/articles/PMC3576830/

NASA (2020) Prediction of worldwide energy resource (POWER). Climatology Resource for SSE-Renewable Energy. https://power.larc.nasa.gov/data-access-viewer/. Accessed 12 July 2026

NOAA CPC (2025) Oceanic Niño Index (ONI). https://origin.cpc.ncep.noaa.gov/products/analysis_monitoring/ensostuff/ONI_v5.php. Accessed 15 July 2026

NOAA PSL (2025) Dipole Mode Index (DMI). https://psl.noaa.gov/gcos_wgsp/Timeseries/DMI/. Accessed 15 July 2026

963 Nguvava M, Abiodun BJ (2023) Potential impacts of 1.5 °C and 2 °C global warming levels on
964 drought modes over Eastern Africa. Clim Change 176:163.
965 https://doi.org/10.1007/s10584-023-03631-z.
966 Nicholson SE (2017) Climate and climatic variability of rainfall over eastern Africa. Rev Geophys
967 55:590–635. DOI: 10.1002/2016RG000544
968 Nsubuga FNW, Olwoch JM, De Rautenbach CJW, Botai OJ (2014) Analysis of Mid-Twentieth
969 Century Rainfall Trends and Variability over Southwestern Uganda. Theor Appl Climatol
970 115:53-71. https://doi.org/10.1007/s00704-013-0864-6
971 Ojara MA, Namumbya S, Ogwang BA, Limbu PTS (2024) Regional and farm level droughts
972 characteristics for southwestern Uganda during 1981–2017. Soil Security 15:100148.
973 https://doi.org/10.1016/j.soisec.2024.100148
974 Omondi OA, Lin Z (2023) Trend and spatial-temporal variation of drought characteristics over
975 equatorial East Africa during the last 120 years. Front Earth Sci 10:1064940.
976 https://doi.org/10.3389/feart.2022.1064940
977 Onyutha C (2016) Geospatial trends and decadal anomalies in extreme rainfall over Uganda, East
978 Africa. Adv Meteorol 2016:6935912. https://doi.org/10.1155/2016/6935912
979 Ouhamdouch S, Bahir M, Ouazar D, Goumih A, Zouari K (2020) Assessment of the Climate
980 Change Impact on the Future Evapotranspiration and Flows from a Semiarid Environment.
981 Arab J Geosci 13:82. https://doi.org/10.1007/s12517-020-5065-x.
982 Palmer PI, Wainwright CM, Dong B *et al (2023)* Drivers and impacts of Eastern African rainfall
983 variability. Nat Rev Earth Environ 4:254–270. https://doi.org/10.1038/s43017-023-00397-
984 x
985 Pettitt AN (1979) A non-parametric approach to the change-point problem. J R Stat Soc Ser C
986 (Appl Stat) 28(2):126-135. https://doi.org/10.2307/2346729
987 Roy I, Troccoli A (2024) Important drivers of East African monsoon variability and improving
988 rainy season onset prediction. Nat Hazards 120:429–445. https://doi.org/10.1007/s11069-
989 023-06223-3
990 Saji NH, Goswami BN, Vinayachandran PN, Yamagata T (1999) A dipole mode in the tropical
991 Indian Ocean. Nature 401:360–363. https://doi.org/10.1038/43854
992 Schober P, Boer C, Schwarte LA (2018) Correlation Coefficients: Appropriate Use and
993 Interpretation. Anesth Analg 126(5):1763–1768.
994 https://doi.org/10.1213/ANE.0000000000002864

995 Schwarzwald K, Seager R (2024) Revisiting the East African paradox: CMIP6 models also
996 struggle to reproduce strong observed long-rain drying trends. J Clim 37(24):6311-6329.
997 https://doi.org/10.1175/JCLI-D-24-0225.1
998 Sen PK (1968) Estimates of the regression coefficient based on Kendall's tau. J Am Stat Assoc
999 63:1379–1389. https://doi.org/10.1080/01621459.1968.10480934
1000 Some'e BS, Ezani A, Tabari H (2013) Spatiotemporal Trends of Aridity Index in Arid and Semi-
1001 Arid Regions of Iran. Theor Appl Climatol 111:149-160. https://doi.org/10.1007/s00704-
1002 012-0650-x.
1003 Spinoni J, Vogt J, Naumann G, Barbosa P, Dosio A (2018) Will drought events become more
1004 frequent and severe in Europe? Int J Climatol 38:1718-1736.
1005 https://doi.org/10.1002/joc.5291
1006 Tan F, Liu R, Wu M, Chen J, Ye Z (2026) Drought-heatwave compound events in China: Long-
1007 term changes, regional drivers, and rising event probability. J Geophys Res Atmos
1008 131(12):e2026JD046972. https://doi.org/10.1029/2026JD046972
1009 Taye MT, Dyer E (2024) Hydrologic extremes in a changing climate: A review of extremes in East
1010 Africa. Curr Clim Change Rep 10(1):1–11. https://doi.org/10.1007/s40641-024-00193-9
1011 Theil H (1950) A Rank-Invariant Method of Linear and Polynomial Regression Analysis.
1012 Nederlandse Akademie Wetenschappen Series A 53:386-392
1013 Tibara Y, Wasswa H, Semakula HM (2023) Vulnerability assessment to flood hazards of
1014 households in flood-prone areas of Kasese District, Western Uganda. World Water Policy
1015 9(2):221–241. https://doi.org/10.1002/wwp2.12098.
1016 Thornthwaite CW (1948) An approach toward a rational classification of climate. Geogr Rev
1017 38:55–94. https://doi.org/10.2307/210739.
1018 Tilahun M, Tesfamichael SG, Sasaki T, Angassa A (2026) Topographic modulation of drought
1019 propagation establishes low-elevation hotspots and mid-elevation climatic refugia in
1020 Southern Africa. *Ecol Indic* 185:114807. https://doi.org/10.1016/j.ecolind.2026.114807.
1021 Uganda Bureau of Statistics (UBOS) (2017) National Population and Housing Census 2014: Area
1022 Specific Profile Series - Kasese District. UBOS, Kampala
1023 Uwimbabazi J, Jing Y, Iyakaremye V, Ullah I, Ayugi B (2022) Observed changes in
1024 meteorological drought events during 1981–2020 over Rwanda, East Africa. Sustainability
1025 14(3):1519. https://doi.org/10.3390/su14031519.

Van Loon AF (2015) Hydrological drought explained. WIREs Water 2:359–392. https://doi.org/10.1002/wat2.1075.

Vicente-Serrano SM, Beguería S, López-Moreno JI (2010) A multiscalar drought index sensitive to global warming: The Standardized Precipitation Evapotranspiration Index. J Clim 23:1696–1718. https://doi.org/10.1175/2009JCLI2909.1

Vicente-Serrano SM, López-Moreno JI, Drumond A, Gimeno L, Nieto R, Morán-Tejeda E, Zabalza J (2011) Effects of warming processes on droughts and water resources in the NW Iberian Peninsula (1930−2006). Clim Res 48(2-3):203-212. https://doi.org/10.3354/cr01002

Vicente-Serrano SM, López-Moreno JI, Gimeno L, Nieto R, Morán-Tejeda E, Lorenzo-Lacruz J, Beguería S, Azorin-Molina C (2011a) A multiscalar global evaluation of the impact of ENSO on droughts. J Geophys Res Atmos 116:D20109. https://doi.org/10.1029/2011JD016039

Wainwright HM, Dafflon B, Siirila-Woodburn ER (2024) Model and remote-sensing-guided experimental design and hypothesis generation for monitoring snow-soil-plant interactions. Front Water 6:1220146. https://doi.org/10.3389/frwa.2023.1220146

Wibawanty DR, Supari, Santikayasa IP (2026) Characterisation and regionalization of dry spells across Java-Indonesia using relative frequency and fractional contribution to total duration. Front Clim 8:1937736. https://doi.org/10.3389/fclim.2026.1937736

World Meteorological Organization (WMO) (2025) State of the Climate in Africa 2024 (WMO-NO. 1370). WMO, Geneva. https://library.wmo.int/idurl/4/69495

Xie P, Gu H, Sang YF, Wu Z, Singh VP (2019) Comparison of different methods for detecting change points in hydroclimatic time series. J Hydrol 577:123973. https://doi.org/10.1016/j.jhydrol.2019.123973

Yuan X, Wang Y, Ji P, Wu P, Sheffield J, Otkin JA (2023) A global transition to flash droughts under climate change. Science 380(6641):187-191. https://doi.org/10.1126/science.abn6301

Yue S, Pilon P (2004) A comparison of the power of the t test, Mann–Kendall, and bootstrap tests for trend detection. Hydrol Sci J 49:21–37. https://doi.org/10.1623/hysj.49.1.21.53969

Zheng Y, Tam CY, Collins M (2025) Indian Ocean Dipole impacts on Eastern African short rains across observations, historical simulations and future projections. Earth's Future 13:e2024EF005219. https://doi.org/10.1029/2024EF005219